

How To Measure Knocking Intensity In Dual-Fuel Internal Combustion Engines : A Review

Dany Iman Santoso¹

(Received: 19 February 2025 / Revised: 10 March 2025 / Accepted: 15 March 2025 / Available Online: 21 March 2025)

Abstract— Internal combustion engines (ICE), especially diesel engines, require additional (secondary) fuel to improve their gas emissions. The selection of hydrogen as a secondary fuel in a diesel dual fuel (DDF) system is meaningful because it does not contain carbon to support exhaust gas decarbonization. Hydrogen also has a high calorific value, which can be a threat of knocking in the engine during operation. Early detection of knocking can prevent further damage to the piston and cylinder. Experts apply pressure and frequency calculations to measure the intensity of knocking. The results obtained in a homogeneous charge compression ignition (HCCI) engine were that slight knocking occurred at a hydrogen-air ratio above 0.3, and heavy knocking rose at a hydrogen-air ratio of 0.45.

Keywords—internal combustion engine, diesel engine, decarbonization, hydrogen, diesel dual fuel, knocking intensity.

I. INTRODUCTION

Environmental issues related to global warming and the dwindling reserves of fossil fuels make alternative fuels a solution to reduce exhaust emissions from internal combustion engines (ICEs) [1]. ICEs are still the mainstay of the transportation system, especially for heavy-duty vehicles such as trucks, marine, and aviation, although electric vehicles have developed as an alternative [2]. The alternative fuels used are usually compressed natural gas (CNG) which has a high-octane number because the stoichiometric operation of CNG can approach low emissions and high performance [3]. Another popular one is hydrogen which has a high combustion rate and is carbon-free [4]. Current uses of hydrogen are fuel cells (FCs) and ICEs, but many prefer ICEs because of their higher efficiency at high loads [5].

ICEs using hydrogen fall into two clusters: those that burn hydrogen alone and those that add it in dual fuel mode [6]. Using high-octane fuel is a strategy to avoid auto-ignition while improving performance [7]. However, severe thermodynamic conditions can cause auto-ignition before the first ignition in spark ignition (SI) and after the first ignition in compression ignition (CI) [8]. Incorrect auto ignition with ignition timing of the combustion process causes knocking [9]. Knocking is a strong local pressure that includes pressure oscillations with substantial amplitude and can cause serious damage to the engine [10].

The study of knocking during the combustion process in ICE is critical because it is related to performance, durability, and fuel consumption [11]. Manufacturers avoid the occurrence of a super knock because the pressure amplitude can reach 200 bar when it occurs [12]. It can damage the piston, valve, spark plug (in SI),

and injector nozzle (in CI) in a short period [13]. The knocking analysis method uses cylinder pressure from sensor measurements during the combustion process [14]. In addition, another method is frequency analysis which captures the frequency spectrum of pressure oscillations reasoned by knocking [15].

The following sub-chapters in this review will present knocking variations based on their cylinder pressure rise. The next chapter provides methods for analyzing knocking intensity based on pressure and frequency. This chapter also offers the steps to calculate knocking intensity based on the cylinder pressure graph. The next chapter allows knocking analysis in a homogeneous charge compression ignition (HCCI) engine with a compression ratio (CR) of 26 and a variation of the air hydrogen ratio from 0.23 to 0.45. This analysis involves the cylinder pressure rise rate (PRR) and the frequency caused by knocking.

A. Slight and normal knock

The combustion analyzer measures in-cylinder pressure (ICP) and pressure rise rate (PRR) due to fuel combustion in the combustion chamber. The PRR result is usually in the form of pressure oscillations, and the amplitude of the oscillations distinguishes the types of knocks [16]. A slight knock is a small explosion that accompanies the fuel combustion process. There will be a place with a high fuel concentration in the combustion chamber when fuel is injected. A slight knock occurs due to auto-ignition from the spread of fuel in other areas that are not fuel concentration places and usually has an amplitude of less than 1 bar, as shown in Figure 1a [17].

Normal knock occurs because the fuel distribution in other areas is higher in concentration than a slight knock, so the resulting explosion is stronger also. The amplitude of normal knock is usually still below 10 bar, as presented in Figure 1b [18] [19] [20]. Normal knock commonly occurs in ICE and helps to improve engine performance. The engine cannot avoid normal knock because fuel spreads in the combustion chamber naturally and experiences auto-ignition naturally.

Dany Iman Santoso, Faculty of Engineering, Universitas Negeri Surabaya, Surabaya, 60231, Indonesia. E-mail: danyisantoso@unesa.ac.id

B. Heavy and super knock

A heavy knock is a knock that can cause damage if left for a long time. Heavy knocking generally occurs because the fuel ignites quickly before the combustion process comes in SI engines. Meanwhile, in CI engines, it typically happens because the ignition delay is too long. Low research octane number (RON) excuses the fuel to ignite shortly and high fuel concentration reasons a long ignition delay. The amplitude of pressure oscillation in heavy knock can reach above 10 bar, as illustrated in Figure 2a, which results in a knocking sound that can be heard [21].

A super knock is a knock that can reach a pressure oscillation amplitude above 100 bar, as described in Figure 2b [22]. It can rise because all the fuel cannot withstand the pressure in the combustion chamber which has a high compression ratio in the SI engine. A high fuel concentration has not been burned causing an ignition delay in the CI engine. Once burned, a large explosion follows and can damage spare parts instantly.

II. METHOD

A. Cylinder pressure

PRR measurement in the combustion process is usually the basis for compiling conventional knock matrices, as presented in Table 1. These matrices base their measurements on the largest amplitude on the PRR graph or band-pass filtered signal (p_{fit}). Some matrices that do this are MAPO, IMPO, and AE. Meanwhile, MVTD uses the third derivative of the band-pass filtered signal to calculate the knock intensity (KI). In addition to using the PRR graph, conventional knock matrices also use the heat release rate (HRR) graph to calculate KI.

The simple formula for KI analysis using the MAPO, IMPO, and AE methods is the difference between the

$$dp(\theta) = \frac{1}{1118d\theta} [86(p_{i-4} - p_{i+4}) + 126(p_{i+1} - p_{i-1})] \quad (2)$$

$$dp(\theta) = \frac{1}{33(1118d\theta)^3} [1272112(p_{i-16} - p_{i+16}) + 4393224(p_{i+15} - p_{i-15}) + 5067808(p_{i+14} - p_{i-14}) + 10302620(p_{i-13} - p_{i+13}) + 30889588(p_{i-12} - p_{i+12}) + 31167114(p_{i-11} - p_{i+11}) + 19489100(p_{i+10} - p_{i-10}) + 120235553(p_{i+9} - p_{i-9}) + 225356606(p_{i+8} - p_{i-8}) + 223838505(p_{i+7} - p_{i-7}) + 77354261(p_{i+6} - p_{i-6}) + 149585072(p_{i-5} - p_{i+5}) + 352659296(p_{i-4} - p_{i+4}) + 431730834(p_{i-3} - p_{i+3}) + 365576347(p_{i-2} - p_{i+2}) + 194997696(p_{i-1} - p_{i+1})] \quad (3)$$

The HRR method is the first derivation of the heat (Q) equation as a function of crank angle (θ), as depicted in Equation (4) [28] [29].

$$\frac{dQ}{d\theta} = \frac{\gamma}{\gamma-1} p \frac{dV}{d\theta} + \frac{1}{\gamma-1} V \frac{dp}{d\theta} \quad (4)$$

where V is the volume of the cylinder, and γ is the specific heat ratio, which has a value of 1.4 for air.

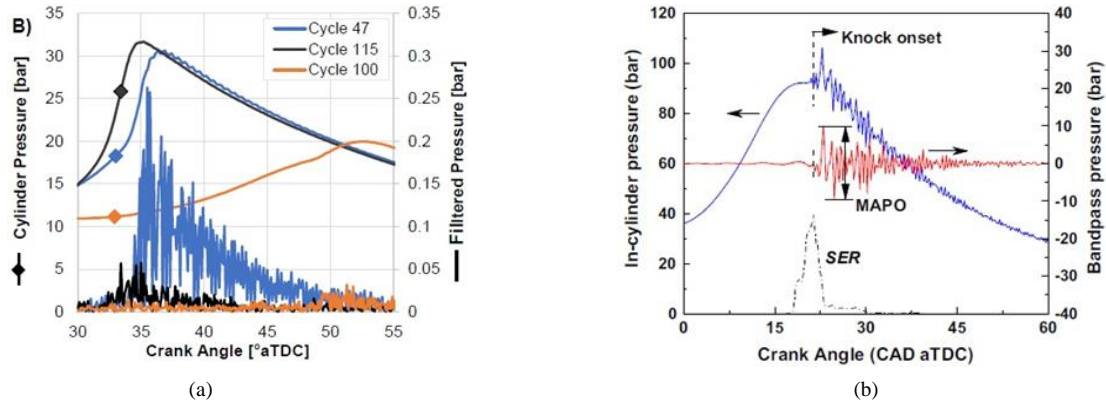


Figure 1. Bandpass filtered: (a) Slight knock signals and (b) Normal knock signals.

maximum (p_{max}) and minimum (p_{min}) filtered pressure, as presented in Equation (1) [23] [24].

$$MAPO = p_{max} - p_{min} \quad (1)$$

As for MVTD, they have a pressure (p) equation as a function of crank angle (θ), as described in Equation (2) [25][26], and its third derivative, as shown in Equation (3) [27].

B. Ringing intensity

The ringing intensity (RI) method measures knock using cylinder pressure data, as illustrated in Equation (5) [30]. RI limits knock to 5 MW/m², which is the sound that can be heard by the human ear when knocking occurs. Researchers rarely use this method because the limit value is high, and it only relies on cylinder pressure data without knowing the frequency data of the sound.

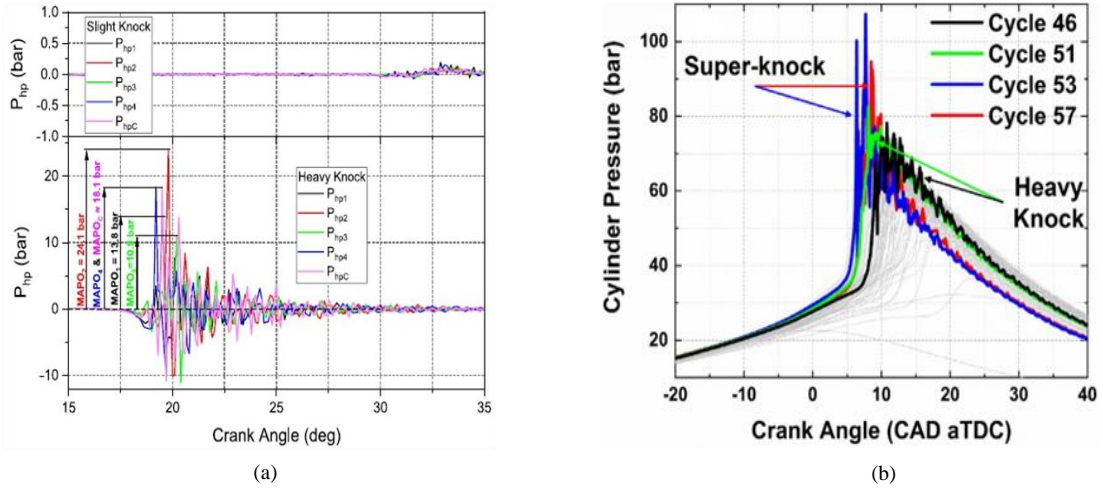


Figure. 2. (a) Filtered pressure signals (P_{hp}) for slight and heavy knock and (b) Heavy and super knock signals.

$$RI = \frac{\sqrt{\gamma RT_{\max}}}{2\gamma P_{\max}} \left[\beta \left(\frac{dp}{d\theta} \right)_{\max} \right]^2 \quad (5)$$

where R is the universal gas constant, T is the in-cylinder temperature, and β is a tuning parameter (0.05).

C. Resonance frequency

The mechanism of the components inside the cylinder causes the resonance of the cylinder pressure, as given in Table 2 [31]. The sound sensor attaches to the outer wall of the cylinder and captures the value of this frequency. When knocking rises, the spectrogram catches the frequency measured by the short-time Fourier transform (STFT), as represented in Figure 3. Knocking causes the appearance of several narrow bands in the spectrogram. Assuming the cylinder space can estimate the resonance

the Draper Equation [31].

$$f_{(i,j)} = c \sqrt{\left(\frac{B_{(i,j)}}{\pi D} \right)^2 + \left(\frac{g}{2h} \right)^2} \quad (6)$$

$$f_{(i,j)} = c \frac{B_{(i,j)}}{\pi D} \quad (7)$$

For mode (1,0), Equation (7) with some adjustments to Equations (8) and (9) will become Equation (10) [31].

$$xc = \sqrt{\gamma RT} \quad (8)$$

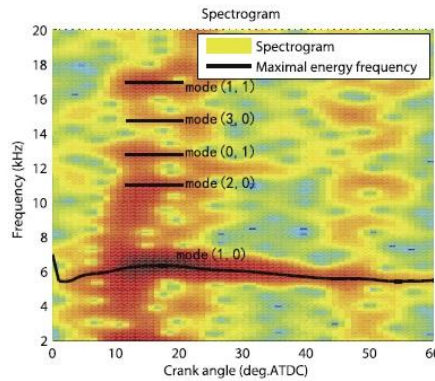


Figure. 3. Spectrogram and resonance mode.

frequency by solving the wave equation using the Bessel function. The resonance frequency depends on the mode, cylinder geometry, and combustion parameters.

Equation (6) gives the formula for calculating the resonant frequency where f is the frequency, c is the speed of sound, D is the cylinder diameter, g is the axial mode, and h is the cylinder height. i and j are the number of circumferential pressure modes and the number of radial pressure modes, respectively. B is the Bessel constant, and the values are presented in Table 3. The simplification of Equation (6) in Equation (7) is called

$$RT = \frac{pV}{m} \quad (9)$$

$$f_{res} = \frac{\alpha B_{(i,j)}}{\pi D} \sqrt{\frac{pV}{m}} \quad (10)$$

Where α and m are the Bessel shifting factor and trapped mass, respectively.

Bessel shifting factor is related to calibration due to the influence of crank shift, as mentioned in Equation (11).

The researchers calibrated the shifting factor for each crank angle using offline data when knocking occurred in the cycle. The researchers also calculated the trapped mass when performing the calibration.

$$\alpha(\theta) = f_{res}(\theta) \frac{\pi D}{B_{(1,0)}} \sqrt{\frac{m}{\gamma(\theta) p(\theta) V(\theta)}} \quad (11)$$

The drum mode prediction, as shown in Table 4 [32], provides a diagrammatic representation of the mode at which the beats occur along with their minimum frequency values.

D. Knocking intensity calculations

Accurate calculation of KI through two calibration stages, offline calibration and online estimation, as described in Figure 4 [31]. This method combines cylinder pressure and resonance frequency data. Offline calibration calibrates the Bessel shift constant from the cylinder pressure data. The result of this stage obtains the correct diagram mode when knocking occurs. This diagram mode determines the estimation of the Bessel constant based on Table 2. After that, the process calculates KI based on the resonance frequency when knocking rose.

Another KI calculation is to calculate the stoichiometric air-fuel ratio (AFR) based on RON, then the cylinder pressure data at that condition is used to calculate MAPO [33]. The calculation of dual fuel AFR requires complex capabilities on chemical reactions, but

cylinder pressure (PCP) and the second rose after [39]. The knock frequency was 3 - 20 kHz, and the average KI value exceeded 0.1 bar [40]. Experiments [41] have shown that the use of cold exhaust gas recirculation (EGR) can reduce knock. Another method to mitigate knock pressure is to mix fuel into dual fuel, which is believed to increase performance [42].

Experiments [43] showed that the water injection could reduce knock on dual fuel hydrogen and natural gas (NG). SI engines with natural gas fuel can reduce knock by adding EGR to the air intake [44]. EGR pressure setting affects the flame shortening and combustion acceleration, which causes an increase in PCP and HRR [45]. Multiple sparks application can reduce knock by reducing pressure spikes and MAPO [46].

Other dual fuel mixtures, such as ammonia and kerosene [47], iso-octane and ammonia [48], n-butanol and natural gas (NG) [49] also experience the same thing as slight knock and knock reduction by the addition of EGR. The shape and size modification of the combustion chamber geometry has little impact on flame development but has a significant effect on flame propagation [50]. Both have different influences on knock due to their flame characteristics.

III. RESULTS AND DISCUSSION

[51] conducted experiments using a homogeneous charge compression ignition (HCCI) engine fueled by diesel and hydrogen. The engine was also a rapid compression expansion machine (RECM) type with a compression ratio (ϵ) between 22 and 32 and a hydrogen-

TABLE I.
CONVENTIONAL KNOCK MATRICES IN KI CALCULATIONS

Metric	Formula
Maximum Amplitude of Pressure Oscillation (MAPO)	$KI = \max \left(\left p_{filt} \right _{\theta_0}^{\theta_0+w} \right)$
Integral of Modulus of Pressure Oscillation (IMPO)	$KI = \max \left(\left p_{filt} \right _{\theta_0}^{\theta_0+w} \right)$
Average Energy (AE)	$KI = \frac{1}{N_s} \cdot \sum_{i=1}^{N_s} p_{filt}^2(i)$
Minimum Value of the Third Derivative (MVTD)	$KI = \min \left(\frac{d^3 p(\theta)}{d\theta^3} \right)$
Heat Release Rate (HRR)	$KI = \sum_{\theta=\theta_{K_0}}^{\theta=\theta_{K_0}+7^\circ CA} \left(\frac{dQ}{d\theta} \right)_{filt}^2 \theta \cdot \Delta\theta$

this is needed when analyzing KI in the combustion process [34]. Heavy knock can occur due to high lambda (actual-stoichiometric AFR ratio) [35]. The higher the lambda, the more homogeneous the fuel mixture will be, thus increasing the possibility of knock [36]. Hydrogen is a fuel that handily activates knock because of its high energy content and burning speed [37].

Hydrogen application as a fuel for Wankel rotary engines also caused knock, which increased engine performance [38]. Knock occurred twice after the top dead center (TDC), where the first appeared before peak

air ratio (ϕ) between 0.23 and 0.45. The results showed that knocking began at ϕ above 0.30, as shown in Figure 5(a). For ϕ below 0.30, in-cylinder pressure did not appear to oscillate.

The increase in cylinder pressure above motoring indicates the beginning of the combustion process. The higher the hydrogen-air ratio, the higher the energy collected, causing more combustion in the cylinder. It causes the increase in cylinder pressure to be high and marked by a steeper pressure gradient.

At $\phi = 0.33$, wavelets emerge, indicating the presence of a knock [52]. The higher the ϕ , the higher the wavelets appear. It is indicated by the increasingly high oscillations in the in-cylinder pressure. These pressure oscillations require bandpass filtering to calculate the intensity of the knock [53].

80 bar can harm the engine. The most effective way to suppress knocking is to prevent the autoignition of the end gases [55].

The bandpass signal filter is called the pressure rise rate (PRR). This PRR indicates the presence of knocking in the engine. The height of the PRR signal underlies the

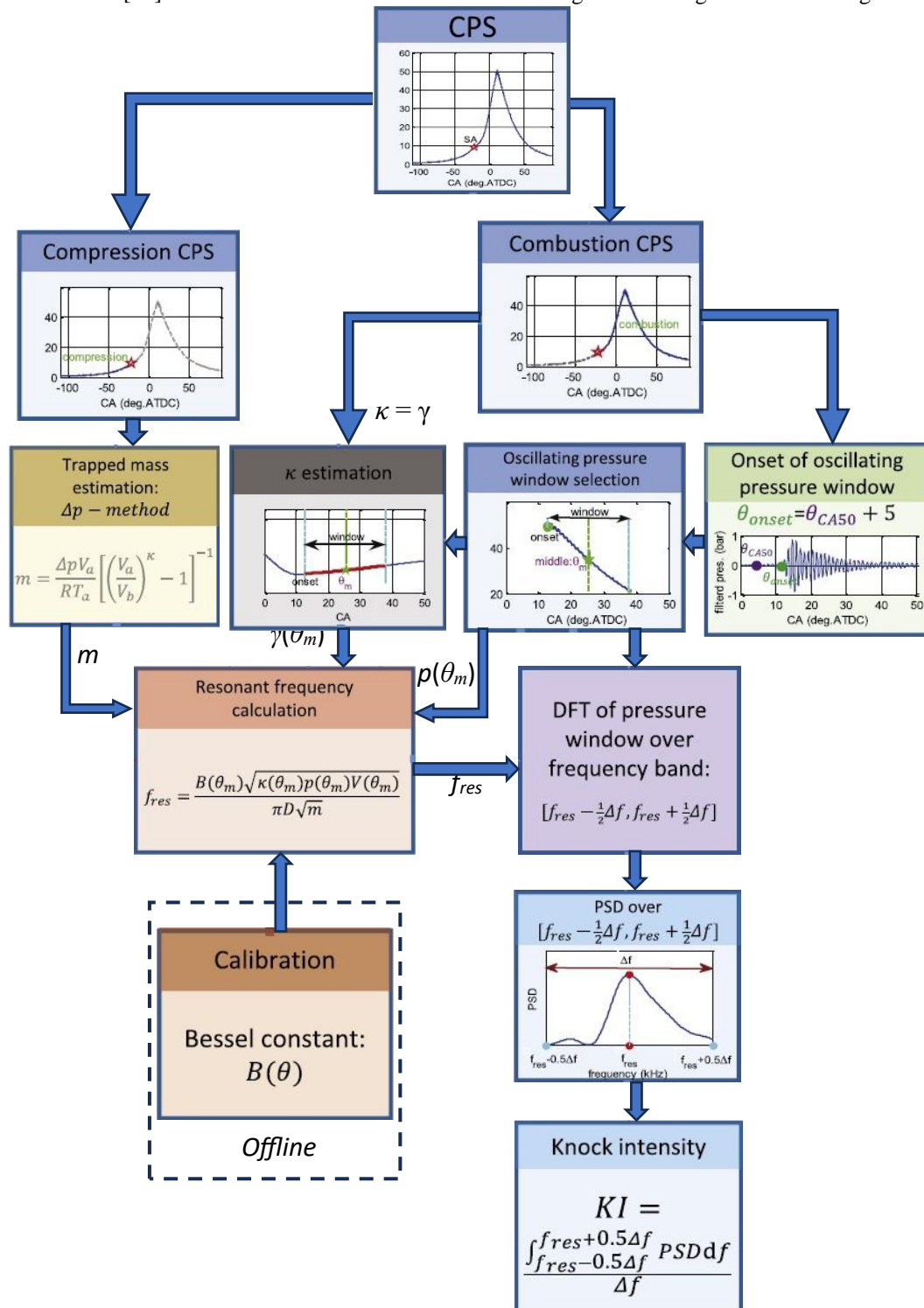


Figure 4. Knock determination process [31].

The filtered bandpass signal is the rate of change of in-cylinder pressure, as presented in Figure 5(b). A KI value of more than 1 bar shows the presence of knock, while a value above 5 bar denotes the presence of light and hard knocks [54]. At $\phi = 0.45$, a KI value of nearly

knocking variation to reach how many bars. At a hydrogen-air ratio of 0.45, although the cylinder pressure shows a pressure of 200 bars, the PRR signal produces 40 bars, which is still in the heavy knock range.

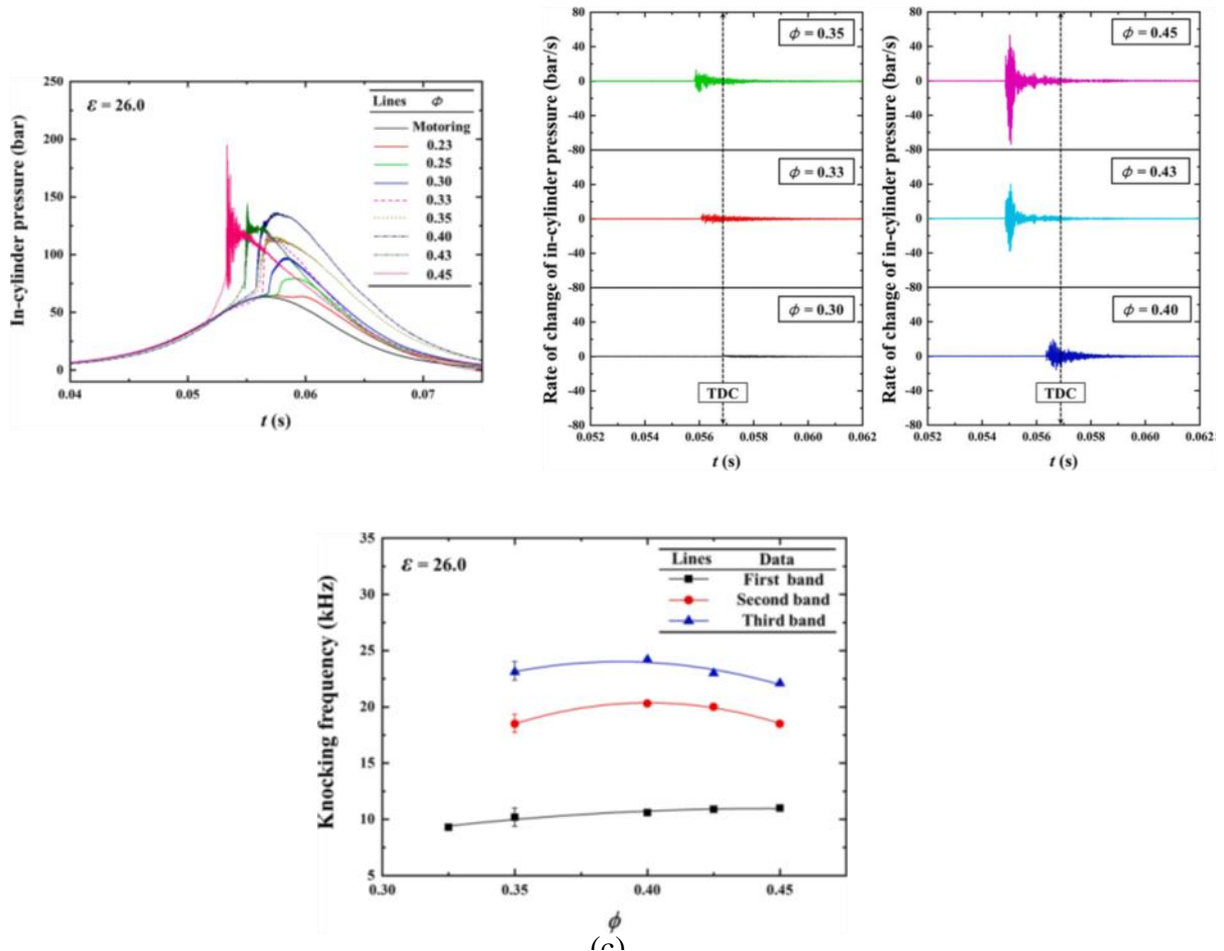


Figure 5. (a) In-cylinder pressure measurement, (b) Bandpass filtered on HCCI engine, and (c) Knocking frequencies with ϕ variations [51]

TABLE 2.
CYLINDER PRESSURE FREQUENCY [31]

Frequency	Description
Low frequency, $f < 0.5$ kHz	The movement of the piston
Medium frequency, $0.3 < f < 2$ kHz	The maximum rate of of pressure rise caused by combustion
High frequency, $f > 3$ kHz	The resonance of the chamber
Noise, $f > 50$ kHz	The piezoelectric pressure sensor behavior

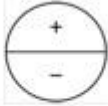
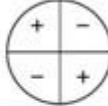
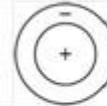
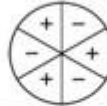

TABLE 3.
BESSEL CONSTANTS [31]

Mode $[i,j]$	Bessel constant $B[i,j]$
[1,0]	1.841
[2,0]	3.054
[0,1]	3.832
[3,0]	4.201
[1,1]	5.332

Knocking in the engine can cause resonant vibrations due to impacts on the cylinder block [56]. It is what

causes the resonance frequency, as provided in Figure 5(c). The resonance frequency can reach above 20 kHz

TABLE 4.
MODES AND RESEMBLING FREQUENCIES [32]

(i,j)	(1,0)	(2,0)	(0,1)	(3,0)	(1,1)
Mode Diagram					
$B_{(i,j)}$	1.841	3.054	3.832	4.201	5.332
$f_{(i,j)}$ (kHz)	6.19	10.27	12.89	14.13	17.94

and is very loud to the human ear. It makes the driver uncomfortable, and frequent knocking can cause lower torque output and higher emissions [57].

The frequency sensor installation on the cylinder also determines the accuracy of the knocking frequency measurement. Some engines have a radiator that covers cylinder heads, causing inaccurate frequency measurements. The first, second, and third bands show that knocking occurs at several frequency ranges and a short time.

IV. CONCLUSION

Dual fuel ICE is the answer to improving combustion performance and reducing emissions, especially greenhouse gases. The most suitable gas fuel is hydrogen because it does not contain carbon and has a high combustion speed. However, using hydrogen in high concentrations can cause knocking in the ICE.

Measurement and calculation of KI on ICE are needed to prevent damage to the engine. Two widely used methods are pressure-based oscillation and frequency-based resonance. Both have their limit for determining the knocking that occurs. If knocking occurs frequently on the engine, it can cause driver discomfort and reduce engine torque.

In an HCCI engine with CR 26 and air hydrogen ratio changes from 0.23 to 0.45, there were several variations of knocking. Slight knocking occurred at an air-hydrogen ratio above 0.3. Heavy knock appeared at an air-hydrogen ratio of 0.45. Slight knock had a cylinder pressure of 100 bar, while heavy knock reached a cylinder pressure of up to 200 bar.

ACKNOWLEDGEMENTS

This manuscript was funded by Lembaga Pengelola Dana Pendidikan (LPDP) through Balai Pembiayaan Pendidikan Tinggi (BPPT).

REFERENCES

- [1] M. D. Altinkurt, M. Merts, M. Tunér, and A. Turkan, "Effects of split diesel injection strategies on combustion, knocking, cyclic variations and emissions of a natural gas-diesel dual fuel medium speed engine," *Fuel*, vol. 347, Sep. 2023, doi: 10.1016/j.fuel.2023.128517.
- [2] X. Zhao, R. Liu, H. Wang, Z. Zheng, and M. Yao, "Effects of charge motion on knocking combustion under boosted high load condition of a medium-duty gasoline engine," *Fuel*, vol. 326, Oct. 2022, doi: 10.1016/j.fuel.2022.125040.
- [3] B. Liang *et al.*, "Effects of chamber geometry, hydrogen ratio and EGR ratio on the combustion process and knocking characters of a HCNG engine at the stoichiometric condition," *Applications in Energy and Combustion Science*, vol. 15, Sep. 2023, doi: 10.1016/j.jaecs.2023.100189.
- [4] H. Meng, C. Ji, J. Yang, K. Chang, G. Xin, and S. Wang, "Experimental understanding of the relationship between combustion/flow/flame velocity and knock in a hydrogen-fueled Wankel rotary engine," *Energy*, vol. 258, Nov. 2022, doi: 10.1016/j.energy.2022.124828.
- [5] F. yu Lai, B. gang Sun, X. Wang, D. sheng Zhang, Q. he Luo, and L. zhi Bao, "Research on the inducing factors and characteristics of knock combustion in a DI hydrogen internal combustion engine

- in the process of improving performance and thermal efficiency," *Int J Hydrogen Energy*, vol. 48, no. 20, pp. 7488–7498, Mar. 2023, doi: 10.1016/j.ijhydene.2022.11.091.
- [6] S. Abubakar *et al.*, "Hydrogen-fuelled internal combustion engines - Bibliometric analysis on research trends, hotspots, and challenges," Apr. 03, 2024, *Elsevier Ltd.* doi: 10.1016/j.ijhydene.2024.02.280.
- [7] M. U. Manzoor, M. R. Yosri, M. Talei, F. Poursadegh, Y. Yang, and M. Brear, "Normal and knocking combustion of hydrogen: A numerical study," *Fuel*, vol. 344, Jul. 2023, doi: 10.1016/j.fuel.2023.128093.
- [8] L. Chen, H. Wei, C. Chen, D. Feng, L. Zhou, and J. Pan, "Numerical investigations on the effects of turbulence intensity on knocking combustion in a downsized gasoline engine," *Energy*, vol. 166, pp. 318–325, Jan. 2019, doi: 10.1016/j.energy.2018.10.058.
- [9] L. Chen, J. Pan, H. Wei, L. Zhou, and J. Hua, "Numerical analysis of knocking characteristics and heat release under different turbulence intensities in a gasoline engine," *Appl Therm Eng*, vol. 159, Aug. 2019, doi: 10.1016/j.applthermaleng.2019.113879.
- [10] J. C. P. Jones and J. Frey, "Closed loop knock intensity characteristics of a classical knock control system," in *IFAC-PapersOnLine*, Sep. 2015, pp. 167–173, doi: 10.1016/j.ifacol.2015.10.024.
- [11] J. Pan, H. Wei, G. Shu, and R. Chen, "Effect of pressure wave disturbance on auto-ignition mode transition and knocking intensity under enclosed conditions," *Combust Flame*, vol. 185, pp. 63–74, 2017, doi: 10.1016/j.combustflame.2017.07.004.
- [12] G. DONG, J. Tian, L. LI, Z. WU, and X. NI, "Study on the ion current forming process under engine knocking conditions," *Combust Flame*, vol. 241, Jul. 2022, doi: 10.1016/j.combustflame.2022.112069.
- [13] H. Xu *et al.*, "Experimental and numerical investigation on effects of pre-ignition positions on knock intensity of hydrogen fuel," *Int J Hydrogen Energy*, vol. 46, no. 52, pp. 26631–26645, Jul. 2021, doi: 10.1016/j.ijhydene.2021.05.154.
- [14] X. Shen and T. Shen, "Knock Limit Controller based on Exponential Moving Average of Knock Intensity," in *IFAC-PapersOnLine*, Elsevier B.V., 2016, pp. 691–695, doi: 10.1016/j.ifacol.2016.08.100.
- [15] M. B. Luong, S. Desai, F. E. Hernández Pérez, R. Sankaran, B. Johansson, and H. G. Im, "A statistical analysis of developing knock intensity in a mixture with temperature inhomogeneitiesR," *Proceedings of the Combustion Institute*, vol. 38, no. 4, pp. 5781–5789, 2021, doi: 10.1016/j.proci.2020.05.044.
- [16] D. Iman Santoso, A. Setiyawan, and B. Sudarmanta, "Possibility of hydrogen gas as the main fuel for diesel engines: A review."
- [17] A. Hoth and C. P. Kolodziej, "Effects of knock intensity measurement technique and fuel chemical composition on the research octane number (RON) of FACE gasolines: Part 1 – Lambda and knock characterization," *Fuel*, vol. 304, p. 120722, Nov. 2021, doi: 10.1016/j.fuel.2021.120722.
- [18] Y. Wu, L. Liu, B. Liu, E. Cao, and Q. Xiong, "Investigation of rapid flame front controlled knock combustion and its suppression in natural gas dual-fuel marine engine," *Energy*, vol. 279, p. 128078, Sep. 2023, doi: 10.1016/j.energy.2023.128078.
- [19] T. Li, T. Yin, and B. Wang, "A phenomenological model of knock intensity in spark-ignition engines," *Energy Convers Manag*, vol. 148, pp. 1233–1247, Sep. 2017, doi: 10.1016/j.enconman.2017.06.078.
- [20] S. Liu, Z. Lin, H. Zhang, N. Lei, Y. Qi, and Z. Wang, "Impact of ammonia addition on knock resistance and combustion

- performance in a gasoline engine with high compression ratio,” *Energy*, vol. 262, p. 125458, Jan. 2023, doi: 10.1016/j.energy.2022.125458.
- [21] Q. Tang *et al.*, “Study of engine knocking combustion using simultaneous high-speed shadowgraph and natural flame luminosity imaging,” *Appl Therm Eng*, vol. 235, p. 121440, Nov. 2023, doi: 10.1016/j.applthermaleng.2023.121440.
- [22] J. Zhang *et al.*, “Prediction of knock intensity and validation in an optical SI engine,” *Combust Flame*, vol. 254, p. 112854, Aug. 2023, doi: 10.1016/j.combustflame.2023.112854.
- [23] W. Zhang, Y. Wang, W. Long, H. Tian, and P. Dong, “Numerical investigation on knock intensity, combustion, and emissions of a heavy-duty natural gas engine with different hydrogen mixing strategies,” *Int J Hydrogen Energy*, vol. 62, pp. 551–561, Apr. 2024, doi: 10.1016/j.ijhydene.2024.03.122.
- [24] Y. Wang *et al.*, “Numerical investigation on combustion regulation for a stoichiometric heavy-duty natural gas engine with hydrogen addition considering knock limitation,” *Int J Hydrogen Energy*, vol. 48, no. 48, pp. 18498–18513, Jun. 2023, doi: 10.1016/j.ijhydene.2023.01.299.
- [25] P. K. Vishnoi, P. S. Gautam, and V. K. Gupta, “The impact on combustion knock in CI engine fueled with methanol-diesel-n-pentanol ternary blends,” *Mater Today Proc*, vol. 52, pp. 1062–1067, 2022, doi: 10.1016/j.matpr.2021.10.491.
- [26] S. Erdoğan, M. K. Balki, and C. Sayin, “The effect on the knock intensity of high viscosity biodiesel use in a DI diesel engine,” *Fuel*, vol. 253, pp. 1162–1167, Oct. 2019, doi: 10.1016/j.fuel.2019.05.114.
- [27] W. Suijs, S. Broekaert, T. De Cuyper, and S. Verhelst, “The sensitivity of pressure-based knock threshold values to alternative fuels: A comparison of methanol vs. gasoline,” *Fuel*, vol. 362, p. 130850, Apr. 2024, doi: 10.1016/j.fuel.2023.130850.
- [28] A. Shere and K. A. Subramanian, “Experimental investigation on effects of equivalence ratio on combustion with knock, performance, and emission characteristics of dimethyl ether fueled CRDI compression ignition engine under homogeneous charge compression ignition mode,” *Fuel*, vol. 322, p. 124048, Aug. 2022, doi: 10.1016/j.fuel.2022.124048.
- [29] A. Shere and K. A. Subramanian, “Effects of hydrogen and EGR on energy efficiency improvement with ultra low emissions in a common rail direct injection compression ignition engine fueled with dimethyl ether (DME) under HCCI mode,” *Int J Hydrogen Energy*, vol. 52, pp. 1447–1474, Jan. 2024, doi: 10.1016/j.ijhydene.2023.08.009.
- [30] C. H. Byun, J. T. Lee, and O. C. Kwon, “An experimental study on the self-ignition and knocking characteristics for hydrogen-fueled homogeneous compression charge ignition engines,” *Fuel*, vol. 351, p. 128970, Nov. 2023, doi: 10.1016/j.fuel.2023.128970.
- [31] X. Shen, Y. Zhang, and T. Shen, “Cylinder pressure resonant frequency cyclic estimation-based knock intensity metric in combustion engines,” *Appl Therm Eng*, vol. 158, p. 113756, Jul. 2019, doi: 10.1016/j.applthermaleng.2019.113756.
- [32] Y. Ye, W. Gao, Y. Li, P. Zhang, and X. Cao, “Numerical study of the effect of injection timing on the knock combustion in a direct-injection hydrogen engine,” *Int J Hydrogen Energy*, vol. 45, no. 51, pp. 27904–27919, Oct. 2020, doi: 10.1016/j.ijhydene.2020.07.117.
- [33] A. Hoth and C. P. Kolodziej, “Effects of knock intensity measurement technique and fuel chemical composition on the research octane number (RON) of FACE gasolines: Part 2 – Effects of spark timing,” *Fuel*, vol. 342, p. 127694, Jun. 2023, doi: 10.1016/j.fuel.2023.127694.
- [34] Q. Duan, X. Yin, X. Wang, H. Kou, and K. Zeng, “Experimental study of knock combustion and direct injection on knock suppression in a high compression ratio methanol engine,” *Fuel*, vol. 311, p. 122505, Mar. 2022, doi: 10.1016/j.fuel.2021.122505.
- [35] H. Feng *et al.*, “Numerical simulation on the effects of n-butanol combined with intake dilution on engine knock,” *Energy*, vol. 271, p. 126918, May 2023, doi: 10.1016/j.energy.2023.126918.
- [36] C. Hong, C. Ji, S. Wang, G. Xin, Y. Qiang, and J. Yang, “Progressive strategies to avoid and exploit knock limit for optimal performance and stoichiometric operation of a DI hydrogen engine with high CR at WOT conditions,” *Fuel*, vol. 357, p. 129849, Feb. 2024, doi: 10.1016/j.fuel.2023.129849.
- [37] Y. Li, W. Gao, P. Zhang, Z. Fu, and X. Cao, “Influence of the equivalence ratio on the knock and performance of a hydrogen direct injection internal combustion engine under different compression ratios,” *Int J Hydrogen Energy*, vol. 46, no. 21, pp. 11982–11993, Mar. 2021, doi: 10.1016/j.ijhydene.2021.01.031.
- [38] H. Meng *et al.*, “Analyzing characteristics of knock in a hydrogen-fueled Wankel rotary engine,” *Energy*, vol. 250, p. 123828, Jul. 2022, doi: 10.1016/j.energy.2022.123828.
- [39] H. Meng, C. Ji, J. Yang, K. Chang, G. Xin, and S. Wang, “A knock study of hydrogen-fueled Wankel rotary engine,” *Fuel*, vol. 321, p. 124121, Aug. 2022, doi: 10.1016/j.fuel.2022.124121.
- [40] H. Meng, C. Ji, J. Yang, G. Xin, and S. Wang, “Statistically discussing impacts of knock type on the heat release process in hydrogen-fueled Wankel rotary engine,” *Int J Hydrogen Energy*, vol. 48, no. 21, pp. 7927–7937, Mar. 2023, doi: 10.1016/j.ijhydene.2022.11.259.
- [41] H. Meng *et al.*, “Analyzing the effects of cooled EGR on the knock of hydrogen-fueled Wankel rotary engine,” *Int J Hydrogen Energy*, vol. 47, no. 77, pp. 33094–33104, Sep. 2022, doi: 10.1016/j.ijhydene.2022.07.185.
- [42] E. Takahashi, Y. Nagano, T. Kitagawa, M. Nishioka, T. Nakamura, and M. Nakano, “Demonstration of knock intensity mitigation through dielectric barrier discharge reformation in an RCEM,” *Combust Flame*, vol. 216, pp. 185–193, Jun. 2020, doi: 10.1016/j.combustflame.2020.02.020.
- [43] X. Wu, K. Liu, Q. Liu, J. Fu, and J. Liu, “Effects of direct water injection timings on knock suppression, combustion, and emission performance of high compression ratio hydrogen-enriched natural gas engine,” *Energy Convers Manag*, vol. 250, p. 114887, Dec. 2021, doi: 10.1016/j.enconman.2021.114887.
- [44] K. Xing, W. Guan, X. Guo, Y. Wang, Z. Tu, and H. Huang, “Potential of high compression ratio combined with knock suppression strategy for improving thermal efficiency of spark ignition stoichiometric natural gas engine,” *Energy Convers Manag*, vol. 276, p. 116544, Jan. 2023, doi: 10.1016/j.enconman.2022.116544.
- [45] K. Luo, Y. Huang, Y. Li, Y. Tao, and Z. Hu, “Effects of high pressure and high-low pressure EGR strategies on the knock tendency, combustion, and performance of a stoichiometric operation natural gas engine,” *Fuel*, vol. 348, p. 128530, Sep. 2023, doi: 10.1016/j.fuel.2023.128530.
- [46] H. Shi, Q. Tang, K. Uddeen, B. Johansson, J. Turner, and G. Magnotti, “Effects of multiple spark ignition on engine knock under different compression ratio and fuel octane number conditions,” *Fuel*, vol. 310, p. 122471, Feb. 2022, doi: 10.1016/j.fuel.2021.122471.
- [47] Z. Liu, F. Liu, H. Wei, and L. Zhou, “Effects of ammonia addition on knock suppression and performance optimization of kerosene engine with a passive pre-chamber,” *Fuel*, vol. 353, p. 129189, Dec. 2023, doi: 10.1016/j.fuel.2023.129189.
- [48] R. Zhang, W. Liu, Q. Zhang, Y. Qi, and Z. Wang, “Auto-ignition and knocking combustion characteristics of iso-octane-ammonia fuel blends in a rapid compression machine,” *Fuel*, vol. 352, p. 129088, Nov. 2023, doi: 10.1016/j.fuel.2023.129088.
- [49] X. Zhen, Z. Tian, Y. Wang, M. Xu, D. Liu, and X. Li, “Knock analysis of bio-butanol in TISI engine based on chemical reaction kinetics,” *Energy*, vol. 239, p. 122190, Jan. 2022, doi: 10.1016/j.energy.2021.122190.
- [50] R. Zou, J. Liu, and N. Wang, “Effect of recess shape on combustion performance and knocking characteristics for a downsized gasoline rotary engine,” *Appl Therm Eng*, vol. 214, p. 118758, Sep. 2022, doi: 10.1016/j.applthermaleng.2022.118758.
- [51] C. H. Byun, J. T. Lee, and O. C. Kwon, “An experimental study on the self-ignition and knocking characteristics for hydrogen-fueled homogeneous compression charge ignition engines,” *Fuel*, vol. 351, p. 128970, Nov. 2023, doi: 10.1016/j.fuel.2023.128970.
- [52] J. Erzy Fiolka, “Publications ESTIMATION OF KNOCK INTENSITY IN SPARK-IGNITION ENGINES BY USING WAVELET TRANSFORM.”
- [53] X. Dou, M. R. Yosri, M. Talei, and Y. Yang, “Impact of wall heat transfer modelling in large-eddy simulation of hydrogen knocking combustion,” *Int J Hydrogen Energy*, vol. 62, pp. 405–417, Apr. 2024, doi: 10.1016/j.ijhydene.2024.03.076.
- [54] Z. Liu, Z. Zhang, S. Rao, and Z. Zheng, “Study of water injection on suppressing knock in a high compression ratio and supercharged hybrid gasoline engine,” *Energy*, vol. 287, Jan. 2024, doi: 10.1016/j.energy.2023.129702.
- [55] W. Liu, Y. Qi, R. Zhang, Q. Zhang, and Z. Wang, “Investigation on end-gas auto-ignition and knock characteristics of iso-octane over wide thermodynamic conditions under jet ignition using a

- rapid compression machine,” *Fuel*, vol. 313, Apr. 2022, doi: 10.1016/j.fuel.2021.122665.
- [56] M. M. Etefagh, M. H. Sadeghi, M. Rezaee, R. Khoshbakhti, and R. Akbarpour, “Application of a new parametric model-based filter to knock intensity measurement,” *Measurement (Lond)*, vol. 43, no. 3, pp. 353–362, Apr. 2010, doi: 10.1016/j.measurement.2009.11.008.
- [57] X. Shen and T. Shen, “Real-time statistical learning-based stochastic knock limit control for spark-ignition engines,” *Appl Therm Eng*, vol. 127, pp. 1518–1529, 2017, doi: 10.1016/j.applthermaleng.2017.08.150.
- [58] W. Suijs, R. De Graeve, and S. Verhelst, “An exploratory study of knock intensity in a large-bore heavy-duty methanol engine,” *Energy Convers Manag*, vol. 302, p. 118089, Feb. 2024, doi: 10.1016/j.enconman.2024.118089.